Journal of ELECTRONIC MATERIALS
DOI: 10.1007/s11664-015-3912-4

Optimization of Thermoelectric Components for Automobile Waste Heat Recovery Systems

SUMEET KUMAR,[1,3] STEPHEN D. HEISTER,[1] XIANFAN XU,[1] and JAMES R. SALVADOR[2]

1.—School of Mechanical Engineering, Purdue University, West Lafayette, IN, USA. 2.—General Motors Global R&D, Warren, MI, USA. 3.—e-mail: kumar94@purdue.edu

For a typical spark ignition engine approximately 40% of available thermal energy is lost as hot exhaust gas. To improve fuel economy, researchers are currently evaluating technology which exploits exhaust stream thermal power by use of thermoelectric generators (TEGs) that operate on the basis of the Seebeck effect. A 5% improvement in fuel economy, achieved by use of TEG output power, is a stated objective for light-duty trucks and personal automobiles. System modeling of thermoelectric (TE) components requires solution of coupled thermal and electric fluxes through the *n* and *p*-type semiconductor legs, given appropriate thermal boundary conditions at the junctions. Such applications have large thermal gradients along the semiconductor legs, and material properties are highly dependent on spatially varying temperature profiles. In this work, one-dimensional heat flux and temperature variations across thermoelectric legs were solved by using an iterative numerical approach to optimize both TE module and TEG designs. Design traits were investigated by assuming use of skutterudite as a thermoelectric material with potential for automotive applications in which exhaust gas and heat exchanger temperatures typically vary from 100°C to over 600°C. Dependence of leg efficiency, thermal fluxes and electric power generation on leg geometry, fill fractions, electric current, thermal boundary conditions, etc., were studied in detail. Optimum leg geometries were computed for a variety of automotive exhaust conditions.

Key words: Thermoelectric generators, waste heat recovery, automotive exhaust, skutterudite, finite difference method

INTRODUCTION

Increasing demand for fuel, limited reserves, and environment concerns serve as motivation to improve the efficiency of energy systems for economical fuel use and reduction of carbon emissions. For a typical automotive vehicle, only 33% of the combustion energy provides recoverable mechanical work spent in delivering piston movement and overcoming pumping losses; the remaining 67% is lost as waste heat. Thirty-seven percent of combustion energy is lost to the engine coolant system and to friction, and 40% (approx. 60% of the waste heat) is dissipated to the environment via hot exhaust gas (Fig. 1).[1] Organic Rankine cycles and thermoelectric generators (TEG) are two major options for exploiting the energy available in exhaust gases. TEGs have several advantages over Rankine cycle generators in that in a TEG there are no moving parts, they are more easily packaged, and have fewer noise, vibration, and harshness issues. TEGs generate power on the basis of the Seebeck effect, a means of direct conversion of waste heat into a usable form of electricity which can meet some vehicle auxiliary power demands and thereby reduce the load the alternator places on the engine. The objective has been to achieve a target of close to 5% improvement in fuel economy for a mid-sized vehicle by use of TEG output power.[2]

(Received February 10, 2015; accepted June 16, 2015)

Published online: 14 July 2015

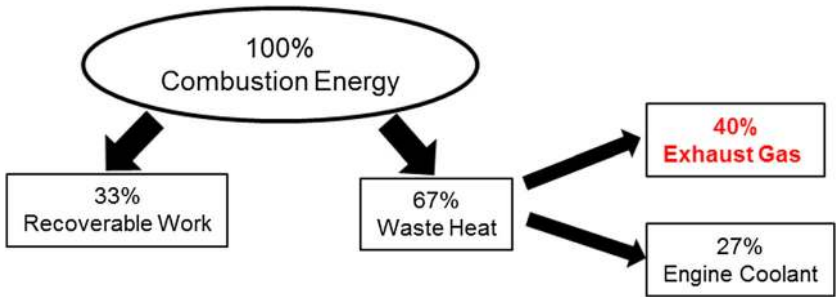

Fig. 1. Energy flow in an internal combustion engine.

The earliest prototypes, dating back to the 1960s, were largely based on Pb–Te and Ge–Bi–Te-based alloys.[3,4] Leading automobile manufacturers, for example Porsche,[5] Nissan Motors,[6] and General Motors,[7,8] have been working on these systems with exhaust gases and engine coolant as the heat source and sink, respectively. However, current projected system efficiencies have been low (typically less than 5%) and mostly hindered by the temperature limitations and power-conversion efficiencies of the thermoelectric materials. Matsubara[9,10] reported a highly efficient thermoelectric stack of TE modules comprising segmented legs produced from highly doped $CoSb_3$ and filled skutterudite RM_4Sb_{12} (R = Ce, Yb; M = Co, Fe, Ni, Pt, Pd) and HZ-14 (based on Bi_2Te_3 from HI-Z Technology), and achieved 5–10% efficiency depending on engine operating conditions. The operating temperature was in the range 350–750°C, and it was suggested that a thermoelectric figure of merit, ZT, of 1.5–2.0 would be needed to achieve 10% overall efficiency. ZT is calculated by use of the formula $ZT = S^2T/\rho\cdot\kappa$, where S is the Seebeck coefficient, ρ the electrical resistivity, κ the thermal conductivity, and T the absolute temperature.

Several analytical and numerical models[11–14] have been used to assess thermoelectric generators, with different levels of sophistication. Espinosa et al.[15] used Mg_2Si/Zn_4Sb_3 for high temperatures and Bi_2Te_3 for low temperatures. This takes into account the temperature-dependence of properties along the heat exchanger but not within the legs. Kumar et al.[16–18] used a thermal resistance network-based model to analyze a thermoelectric generator system for a General Motors prototype generator designed for the Chevrolet Suburban. Junction-averaged thermoelectric properties were used to calculate the Seebeck voltage potential and electrical power.

Optimization of TEGs requires a comprehensive approach which addresses each and every component of a generator system. Use of property-averaging or a similar technique for thermoelectric materials is not sufficient to maximize a generator's performance. The averaging techniques fail to deliver accurate results for thermoelectric modules under high electric current density conditions.[19,20] In addition, these techniques cannot be used for precise optimization of thermoelectric leg geometry, as shown in Appendix A. In these methods, the Thomson coefficient is taken as zero. Also, variation of material properties along the thermoelectric leg height are not taken into account. The high cost of rare-earth elements used in candidate TEM legs is also a prime variable in system trade-off studies.

To address these issues, in this work we focus on modeling the thermoelectric components of a TEG system subjected to conditions characteristic of automobile exhaust. A numerical model is used to study the dependence of electrical power generation on leg height, junction conditions, and area ratio of n-type to p-type materials.[20] The method takes into account temperature-dependent properties along a thermoelectric leg. Mesh independence is verified and the model is used to analyze typical automobiles exhaust conditions. The thermoelectric material in this study is limited to multiple filled skutterudites.[21,22] These materials have desirable ZT values at high temperature making them suitable for applications related to diesel and gasoline engines. Description of the model in the next section is followed by results and conclusions from the study.

NUMERICAL MODELING

The thermal and electrical fluxes through the thermoelectric legs of a TE couple (one n-type leg and one p-type leg) were studied by use of the numerical model of Shih and Hogan.[20] A TE module comprises many such TE couples connected in series electrically and in parallel thermally. The n and p-type legs are divided into segments lengthwise, as shown in Fig. 2. Segment 0 is in contact with the cold side junction and the Nth segment is in contact with the hot side junction. T_H and T_C are hot side and cold side junction temperatures, I is the electric current through the thermoelectric legs, and R_O is the load electrical resistance.

Assuming one-dimensional conduction along the thermoelectric leg, the steady-state energy balance of a thermoelectric element is reduced to Domenicali's equation:[23]

$$\frac{\partial}{\partial x}\left(\kappa(x)\frac{\partial T(x)}{\partial x}\right) = -\rho(x)J^2 + JT(x)\frac{\partial S(x)}{\partial x}, \qquad (1)$$

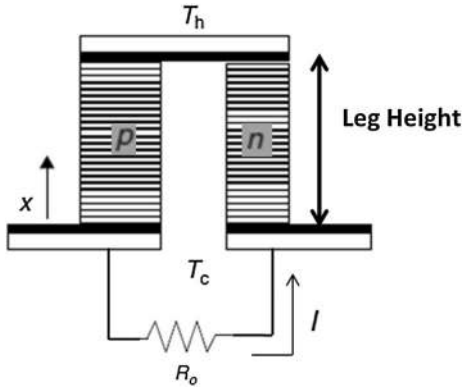

Fig. 2. Schematic diagram of a thermoelectric couple with the legs divided into segments lengthwise.

$$q(x) = JT(x)S(x) - \kappa(x)\frac{\partial T(x)}{\partial x}, \tag{2}$$

where $\kappa(x)$ is the thermal conductivity, $\rho(x)$ is the electrical resistivity, and $S(x)$ is the Seebeck coefficient of the thermoelectric materials as they vary along the leg height dimension x. $T(x)$, $q(x)$ and J are the temperature, heat flux, and current density flux, respectively. In Eq. 1, the term on the left is the Fourier conduction in one dimension, the first term on the right hand is the Joule heating and the last term includes both Peltier (∇S at a junction) and Thomson (∇S in a thermal gradient) effects. In Eq. 2, the first term on the right is the entropy transport term and second term is the thermal conduction.[23] Equation 2 can be substituted in Eq. 1 to derive an equation in terms of heat flux $q(x)$:

$$\frac{\mathrm{d}q(x)}{\mathrm{d}x} = \rho(x)J^2[1 + Z(x)T(x)] - \frac{JS(x)q(x)}{\kappa(x)}, \tag{3}$$

where $Z(x)$ is the figure of merit, given as:

$$Z(x) = \frac{S^2(x)}{\rho(x)\kappa(x)}. \tag{4}$$

Equation 2 can be rearranged to give Eq. 5 as a first order equation in $T(x)$:

$$\frac{\mathrm{d}T(x)}{\mathrm{d}x} = \frac{1}{\kappa(x)}[JT(x)S(x) - q(x)]]. \tag{5}$$

For n-type thermoelectric legs, Eqs. 3 and 5 can be discretized along the height of the leg as a set of algebraic equations represented by Eqs. 6 and 7.[20] The subscript m denotes the mth TE discrete segment, where $m = 0$ and $m = N$, are the segments attached to cold side and hot side junctions respectively. A finite difference method is used to discretize gradient terms by use of the first order forward difference approximation. The prescribed hot side junction T_N (Nth segment) and cold side junction T_0 (0th segment) temperatures serve as boundary conditions. Current density flux through each leg is input to these equations. Because Eqs. 6 and 7 are coupled, they must be solved iteratively to calculate heat fluxes through each TE leg. The properties of thermoelectric legs are averaged over a discrete thermoelectric segment. These calculations are performed for the n and p-type legs of the TE couple.

$$T_{m+1} = T_m + \frac{\mathrm{d}x}{\kappa_m}[JT_mS_m - q_m] \tag{6}$$

$$q_{m+1} = q_m + \left[\rho_m J^2(1 + Z_m T_m) - \frac{JS_m q_m}{\kappa_m}\right]\mathrm{d}x \tag{7}$$

The leg efficiency is the ratio of the electric power generated to the thermal power available at the hot side junction. For the n or p -type leg, this may be expressed as:[20]

$$\eta_{n,p} = \frac{J_{n,p}\left(\int_0^L S_{n,p}(x)\frac{\mathrm{d}T(x)}{\mathrm{d}x}\mathrm{d}x + J_{n,p}\int_0^L \rho_{n,p}(x)\mathrm{d}x\right)}{q_{h_{n,p}}}. \tag{8}$$

The first term in the numerator is the summation of Seebeck potentials along the leg height; the second term is the potential loss because of electric resistance. For a TE couple comprising a single n and single p-type leg, the efficiency can be expressed as:

$$\eta_T = \frac{\eta_p Q_{h_p} + \eta_n Q_{h_n}}{Q_{h_p} + Q_{h_n}} = \frac{\eta_p q_{h_p} A_p + \eta_n q_{h_n} A_n}{q_{h_p} A_p + q_{h_n} A_n} \tag{9}$$

The mesh independence was first verified by assuming a skutterudite module with n-type $Ba_{0.08}La_{0.05}Yb_{0.04}Co_4Sb_{12}$ and p-type $DD_{0.76}Fe_{3.4}Ni_{0.6}Sb_{12}$ TE materials (Fig. 3).[21,22] The leg efficiencies were calculated by use of Eq. 8 for n and p-type skutterudite legs at J_P = 50.9 A/cm2 and $J_N = -37.1$ A/cm^2, respectively. The cold side temperature T_c was fixed at 100°C for calculations throughout this study. The junction temperature difference ΔT ($T_H - T_c$) was set to 450°C and leg height (L_x) as 10 mm. The values J_P = 50.9 A/cm^2 and $J_N = -37.1$ A/cm^2 are the optimum current flux densities for ΔT = 450°C and L_x = 10 mm, as discussed below. The respective leg efficiencies were plotted as a function of increasing number of discrete segments along leg height (mesh size Nx), as shown in Fig. 4. It was found that the solutions varied by less than 0.02% from the finest mesh if a

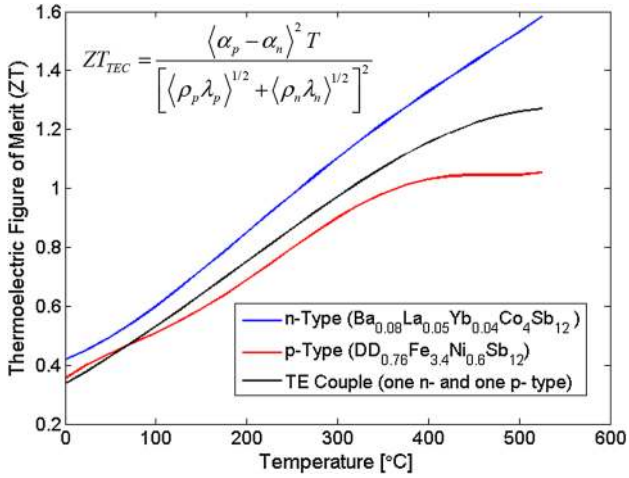

Fig. 3. *ZT* curves for the skutterudites.[21,22]

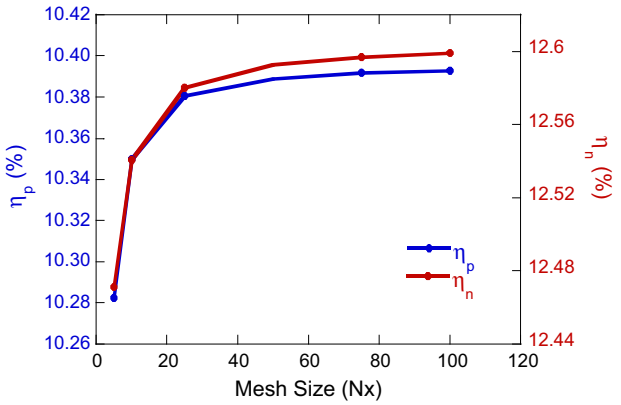

Fig. 4. Mesh independence study for different current density fluxes at $J_P = 50.9$ A/cm^2, $J_N = -37.1$ A/cm^2, $\Delta T = 450$°C, and $L_x = 10$ mm.

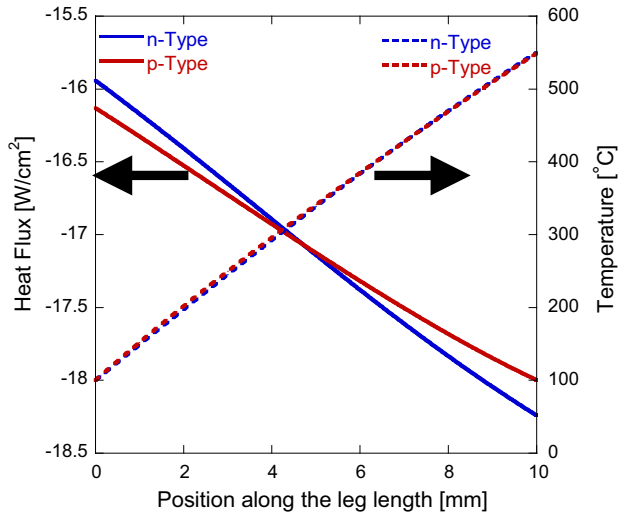

Fig. 5. Heat flux and temperature profiles along the TE legs at $J_P = 50.9$ A/cm^2, $J_N = -37.1$ A/cm^2, $\Delta T = 450$°C, and $L = 10$ mm.

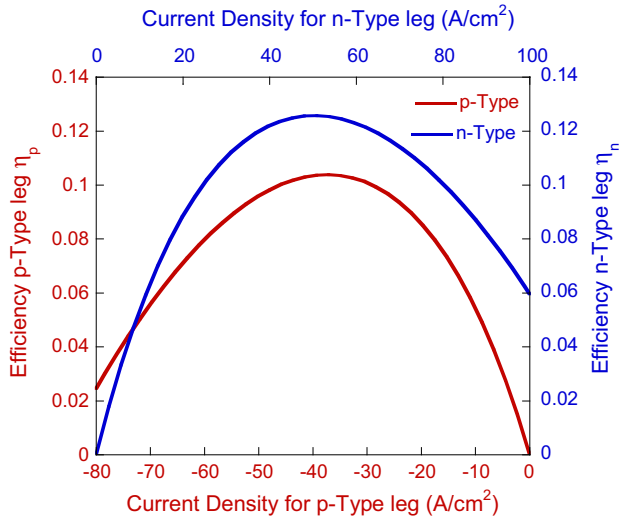

Fig. 6. Leg efficiencies as a function of input current density fluxes with $\Delta T = 450$°C and $L = 10$ mm.

mesh size of 80 was used. A value of $Nx = 500$ was used for the remaining calculations in the paper.

Figure 5 shows the temperature and heat flux profiles along the TE legs. Because material properties are functions of temperature, we observe spatial variations in flux profiles. It should be noted that temperatures of TE segments must match at boundary junctions whereas the respective heat fluxes do not match because input current densities are different.

Equation 8 was used to calculate leg efficiencies for different electric current densities. Figure 6 shows there is an optimum current density for each *n* or *p*-type leg, which can be explained by Eq. 8. The magnitude of the numerator will decrease for lower current densities; the total potential will also decrease with higher current density values however, with increasing electrical resistive potential loss. Table I summarizes the optimum conditions for both types of leg with different hot side and cold side temperature differences; it is worthy of note that *n*-type legs are more efficient than their counterpart *p*-type legs.

THERMOELECTRIC MODULE OPTIMIZATION

As depicted in Fig. 2, the TE couple consists of single *n* and *p*-type TE legs. At steady-state operation the electric current is identical through both legs, so the ratio of cross-sectional area can be represented as $|-J_P A_P| = |J_N A_N| = |I|$. The analysis below emphasizes the effect of conditions such as input current density flux, TE leg area ratio (A_N/A_P), junction temperature, and leg height on the efficiency of the thermoelectric module.

First, the dependence of module efficiency on area ratio was examined. Figure 7 shows the module

Table I. Optimum current densities for skutterudites with leg height L_x = 10 mm

$\Delta T_{\text{Junction}}$ (°C)	$\eta_{\text{Peak},n}$	J_n (Opt.) (A/cm^2)	$\eta_{\text{Peak},p}$	J_p (Opt.) (A/cm^2)
450	0.126	50.32	0.104	−37.34
350	0.101	40.53	0.084	−29.83
250	0.074	30.00	0.061	−21.76
150	0.045	18.64	0.036	−13.26
50	0.015	6.42	0.012	−4.42

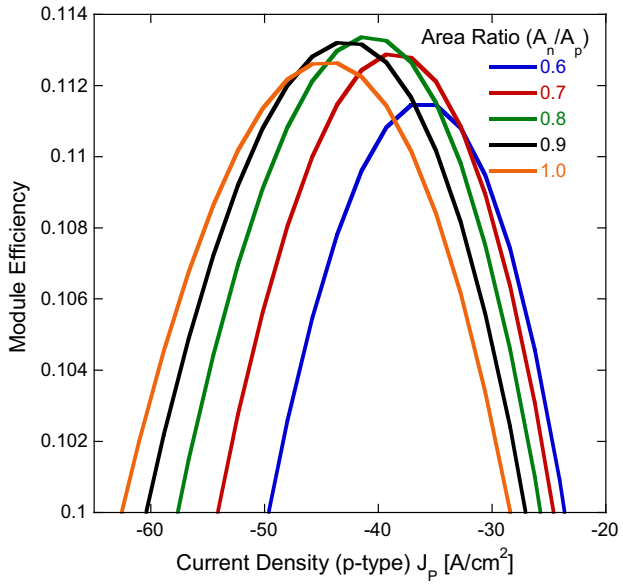

Fig. 7. TE module efficiency as a function of current density at ΔT = 450°C and L_x = 10 mm.

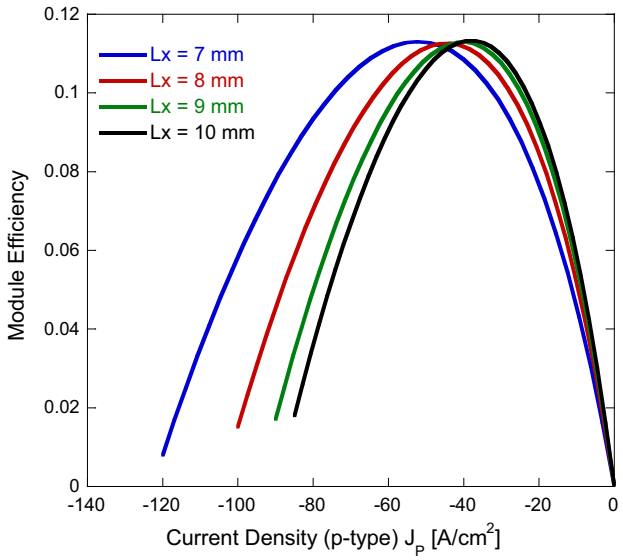

Fig. 8. TE efficiency as a function of J_P for different leg heights at ΔT = 450°C and A_N/A_P = 0.8.

efficiency computed by use of Eq. 9 for different area ratios (A_N/A_P) at ΔT = 450°C and L_x = 10 mm. For skutterudites, the maximum module efficiency (11.33%) occurs at an optimum area ratio of 0.8. Module efficiency (Eq. 9) does not change if the area ratio (A_N/A_P) remains constant which also limits J_N for a given value of J_P. This implies that proper sizing of A_P can help to achieve maximum module efficiency. However, the sizing of A_P (or A_N) will depend on the magnitudes of the electric current and thermal energy.

The variation of TEM efficiency with leg height was studied by fixing the area ratio at 0.8. The results shown in Figs. 8 and 9 reveal the effect of leg height on module efficiency for different current density fluxes and heat fluxes, respectively. An optimum value exists for both these conditions, indicating that leg height cannot be independently optimized without considering local heat transfer conditions within the TEG. Because most TEG designs use a flow-path that subjects TE modules to different temperatures (hottest at inlet and coldest at outlet of TEG), a truly optimum design will

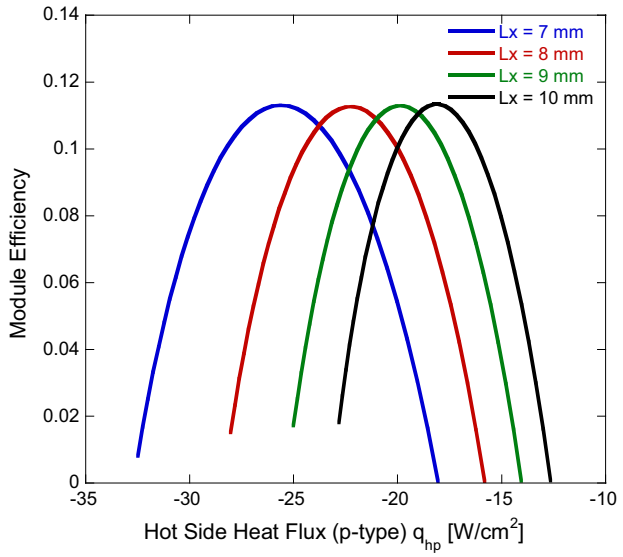

Fig. 9. TE efficiency as a function of hot side heat flux for different leg heights at ΔT = 450°C and A_N/A_P = 0.8.

require different leg heights or fill fractions (discussed below) at different points in the gas path, because of changing heat fluxes during different duty cycles.

Figures 10 and 11 show variation of module efficiency as a function of hot side inputs (J_P, q_{HP}) at L_x = 10 mm and A_N/A_P = 0.8 for different junction temperatures. There is an upper limit for a given ΔT across a TE module. The possible maximum module efficiency decreases with decreasing ΔT across junctions. These plots can be used for thermoelectric module design on the basis of operating conditions (junction temperatures).

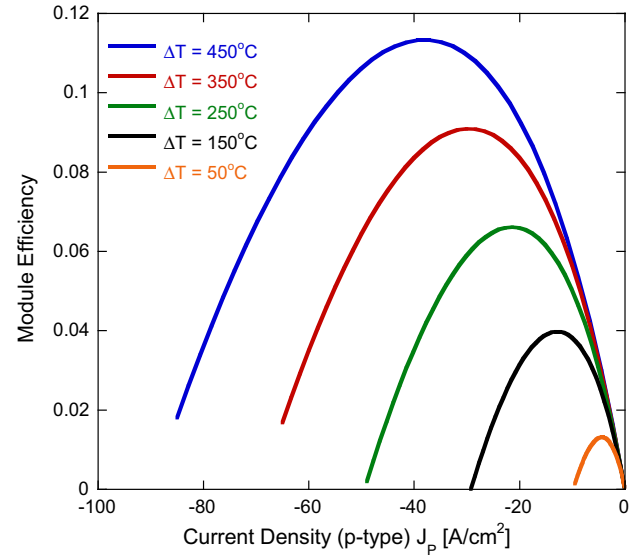

Fig. 10. TE efficiency as a function of J_P for different ΔT at L_x = 10 mm and A_N/A_P = 0.8.

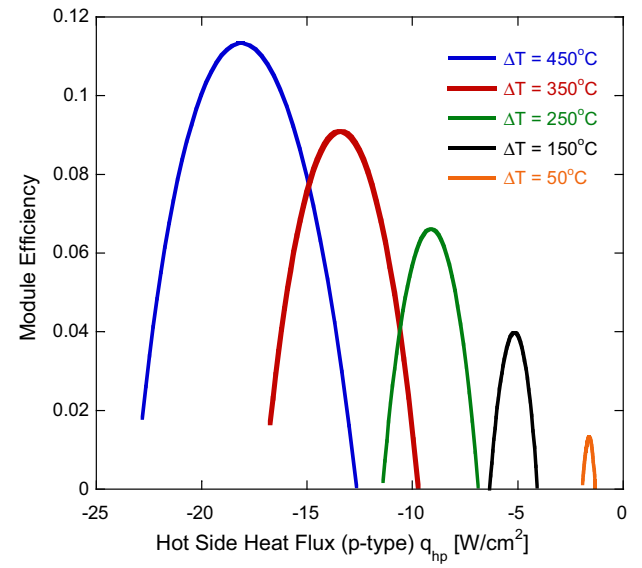

Fig. 11. TE efficiency as a function of hot side heat flux for different ΔT at L_x = 10 mm and A_N/A_P = 0.8.

For the skutterudites used here, maximum module efficiency (11.35%) occurs at an optimum area ratio of 0.8 for the specified conditions ΔT = 450°C and L_x = 10 mm. The cross-sectional areas of the TE legs can be varied without affecting module efficiency as long as the ratio A_N/A_P is constant. For a given A_N/A_P and ΔT, maximum efficiency is attainable at different J_P or q_{HP}. However, maximum possible efficiency is limited by ΔT and decreases with decreasing thermal gradient across junctions (ΔT).

THERMOELECTRIC DESIGN FOR TEG OPTIMIZATION

As already discussed, thermal energy can be extracted from exhaust gas for thermoelectric power generation. Waste heat extraction can be facilitated by allowing a poorly conducting gas to pass through a heat-transfer mechanism, for example a heat exchanger. Peak exhaust gas temperatures lie in the range 550–650°C, providing the thermoelectric modules with a waste heat energy supply of approximately 10 kW for a mid-sized vehicle.[16] The approach used for thermoelectric design of such systems has three stages:

1 the average heat flux is calculated for a given TE module area on the basis of fill fraction;
2 the calculated heat flux is matched to that of a TE module at a given leg height, ΔT, and A_N/A_P; and
3 electric power estimates and volume of TE materials are subsequently calculated.

Here, two scenarios are considered to assess the efficacy of thermoelectric design as represented by Fig. 12. Heat transfer occurs across a heat-exchanger surface of width 0.5 m and length 0.5 m. Case 1 represents configurations in which heat transfer and temperature are uniform at the heat-exchanger surface in a TEG system. In Case 2, the heat transfer and temperature profiles at the surface vary along the direction of flow. For ease of calculation the variation along the flow direction can be visualized as a series of step decrements numbering 1–5, as shown in Fig. 12. One step length is equal to 1/5th of the flow direction length. A specific percentage of the heat transfer area is covered by the thermoelectric legs and is represented by the fill fraction. Ninety percent of the incident thermal energy is assumed to be conducted through the thermoelectric legs, thus generating electrical power. The remaining 10% is assumed to be lost through the conduction in insulators between the TE legs and via radiation losses. The optimum leg area ratio (A_N/A_P) of 0.8 is taken for all subsequent calculations. The cold side junction temperature is approximated as the coolant temperature and kept fixed at 100°C.

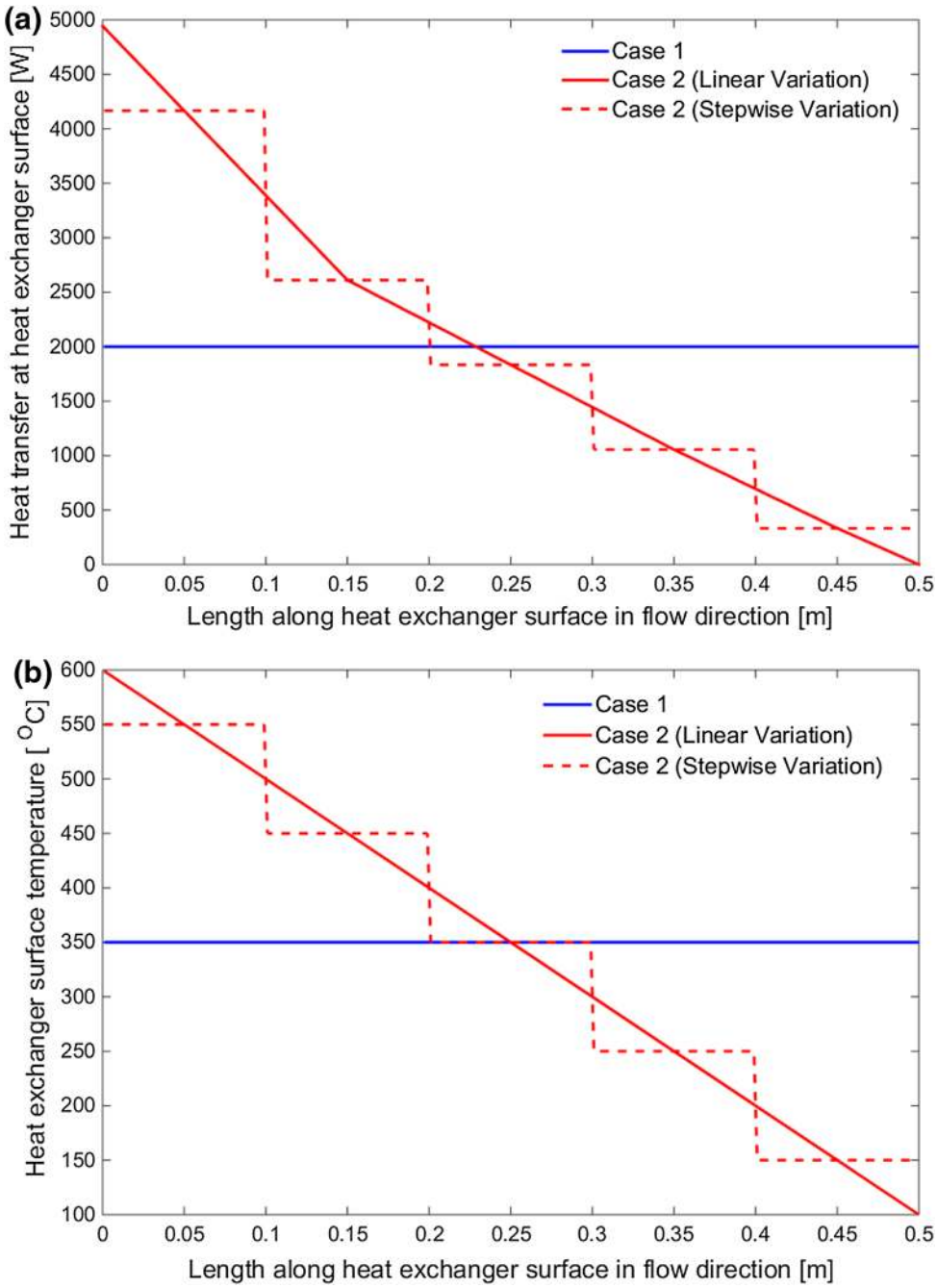

Fig. 12. Variation of heat transfer (a) and temperature (b) over a heat exchanger surface for Case 1 and Case 2. The linear variation is approximated as stepwise profile in five steps for Case 2.

Case 1: Uniform Heat Transfer and Temperature

In this case, there is a uniform supply of 10 kW thermal energy through the exhaust gas over 2500 cm^2 of heat-transfer surface area which is in contact with the hot side surface of thermoelectric modules. For example, after deducting losses and transfer inefficiencies, the average heat flux over the surface is 18 W/cm^2 for a 20% fill fraction and varies with different fill fraction values. A uniform ΔT = 250°C is assumed across TE hot and cold side junctions. Calculations for skutterudite TE modules

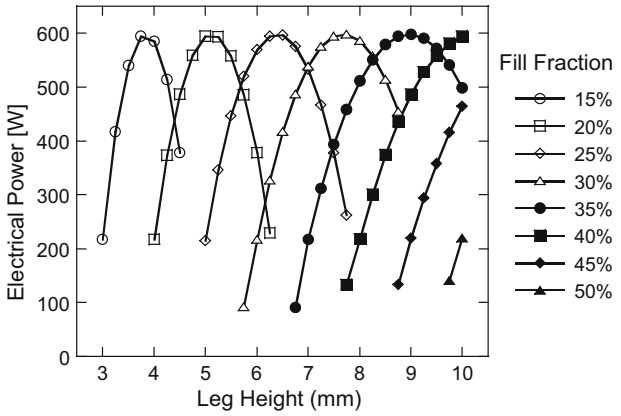

Fig. 13. Electrical power estimates as a function of leg height for Case 1 and different fill fractions, with the area ratio (A_N/A_P) fixed at 0.8 for skutterudite.

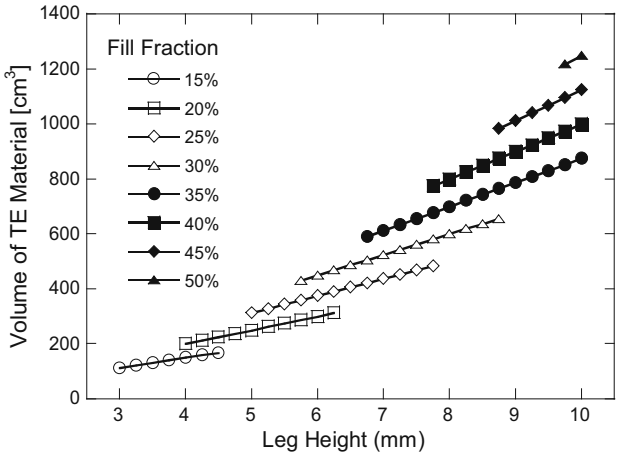

Fig. 14. Required volume of TE materials for Case 1 and different fill fractions.

were performed for a range of TE leg heights and fill fractions. Figure 13 shows the estimated power generation for given thermal energy and surface temperature conditions. Figure 14 shows the volume of TE material required to generate the power that appears in Fig. 13. The fill fraction increases with leg height to match the surface heat flux and generate the same amount of electrical power. This, in turn, increases the volume of TE material
required. For TE modules with a leg height of 3.75 mm and a fill fraction of 15%, generation of 593.8 W electrical power is predicted; 140.6 cm^3 of skutterudite material over 2500 cm^2 heat exchanger area is required.

Case 2: Different Heat Transfer and Temperature

This case mimics transfer in a TEG that has a gas path with successive heat extraction along its length. The heat transfer and temperature profiles are equally distributed area-wise in five steps along the flow direction. Figure 15 shows the electrical power generated for different leg heights (3–10 mm) and optimum fill fraction. The optimum fill fraction along the steps in the flow direction and the total material volumes required are plotted in Fig. 16. The electrical power generation capacity of TE couples decreases substantially along the flow direction and is less than 10 W for Step 5; this is indicative of strong dependence of TE efficiency on junction ΔT. TE modules with a leg height of 4.5 mm and a fill fraction of 20% for Step1 and 15% for Steps 2–5 generate electrical power of 758.9 W; requiring 180.2 cm^3 of TE material. However, the thermoelectric couples in the Step 5 for this configuration only generate 3.39 W of electrical power (Fig. 15).

Table II summarizes the energy distribution and optimum configurations for both cases. The optimum configuration for Case 2 suggests use of a variable fill fraction along flow direction.

CONCLUSIONS

A numerical method has been used to calculate heat transfer and temperature profiles for *n* and *p*-type thermoelectric legs made of filled skutterudite. Leg efficiency was found to be highly dependent on current, junction temperature difference, and leg height. Leg height, fill fraction, and area ratio (A_N/A_P) are important in TEM optimization for any maximum power generation study. However, maximum module efficiency is limited by junction temperatures. An iterative method enables accurate design of optimum TEMs for waste automotive heat recovery. Careful selection of leg height and fill fraction helps achieve maximum electrical power generation while minimizing material requirements. For a fixed heat exchanger surface, and generation of the same amount of power, longer thermoelectric legs require higher fill fractions or larger cross-sectional areas to match the hot side heat flux. This in turn increases the volume of skutterudite required. For the automotive applications considered here (10 kW heat supply over 0.25 m^2 of heat exchanger surface), leg heights in range of 3–5 mm are found to generate the maximum possible electrical power.

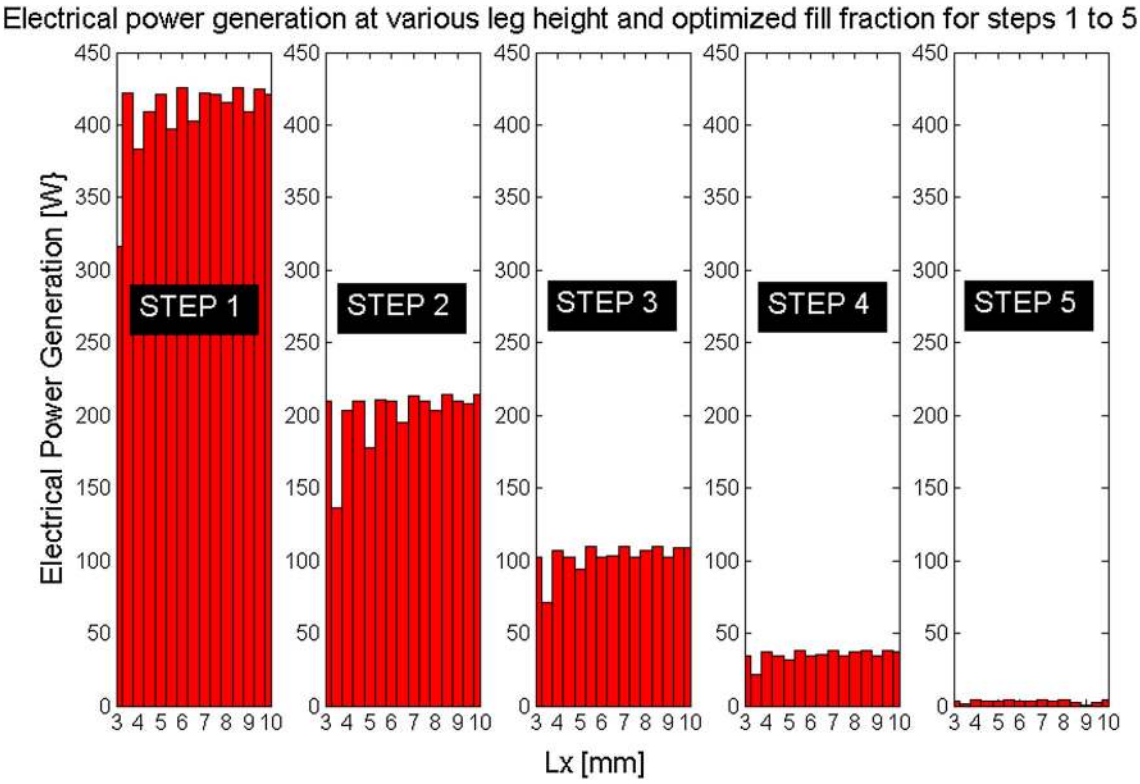

Fig. 15. Electrical power generation for different leg heights, optimum fill fraction, and $A_N/A_P = 0.8$. Steps 1–5 represent each row of TE couples arranged along the flow direction.

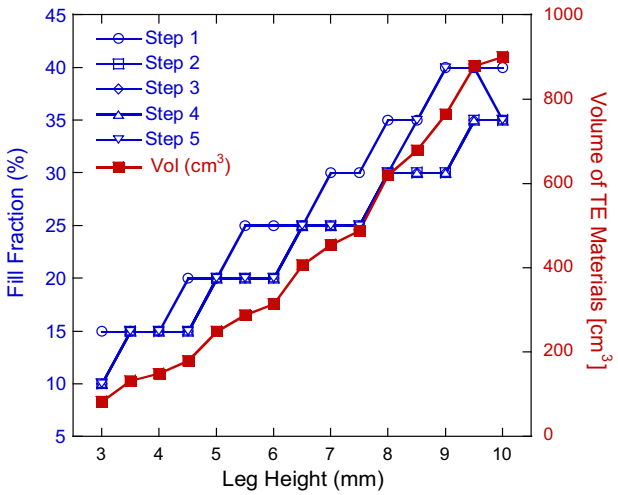

Fig. 16. Optimum fill fractions for different leg heights for Steps 1–5 varying along the flow direction (Case 2). The right hand side axis shows the volume of skutterudite material required.

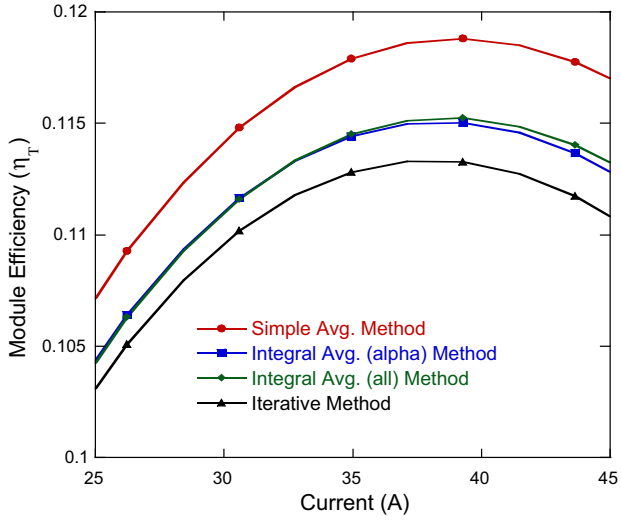

Fig. 17. Method comparison for different current inputs for skutterudites at $L_x = 10$ mm, $A_N/A_P = 0.8$; $\Delta T = 450$°C, and $A_p = 1$ cm^2.

Table II. Electrical power generation for both cases

	Surface heat transfer (kW)	Electrical power (W)	Efficiency (%)	Optimum leg height (mm)	Optimal fill fraction (%)	Volume of skutterudite (cm^3)
Case 1	10.0	593.8	5.9	3.75	15	140.6
Case 2	10.0	758.9	7.6	4.5	20,15,15,15,15	180.2

ACKNOWLEDGEMENTS

This research was made possible by financial support from the National Science Foundation (NSF) and the US Department of Energy (DOE) (CBET-1048616).

APPENDIX A: METHOD COMPARISON

The material properties of thermoelectric legs depend on the temperature. Spatial variation of the temperature lead to large differences in calculated properties if averaging principles are used. The average calculations are performed by use of Eq. 10:

$$\eta_T = \frac{I(\alpha(T_H - T_C) - IR)}{\alpha T_H I + K(T_H - T_C) - 0.5\ I^2 R}. \qquad (10)$$

In this section, a list of such methods is presented and the methods are compared with the iterative method, which has been discussed in detail in previous sections of this paper. The methods of interest are given with a brief description:

1 Simple average method: the leg properties are calculated for the average junction temperature. i.e. $T_M = (T_H + T_c)/2$. For example: $\alpha_{n,p} = \alpha_{n,p}\left(\frac{T_H+T_C}{2}\right)$.

2 Integral average method:

i Integral average (α): Seebeck coefficients only are integral averaged over T_H and T_c. Other properties are calculated for the average junction temperature.

$$\alpha_{n,p} = \frac{\int_{T_C}^{T_H} \alpha_{n,p} dT}{T_H - T_C} \qquad (11)$$

ii Integral average (all): all properties are integral averaged over the junction temperatures.

The simple average method over-predicts efficiency values and does not match the iterative method (Fig. 17). Integral average methods perform better than the simple averaging method but may not be suitable for analysis near the optimum point or for high current values. Simple averaging methods do not take into account the Thomson effect at high currents. The iterative method takes into account variation of material properties; hence the Thomson effect is taken into account for different ranges of input current.

REFERENCES

1. J.R. Salvador, in email conversations dated 18th June, 2014 (2014).
2. J.W. Fairbanks, *2013 Annual Merit Review and Peer Evaluation Meeting*, Washington, DC, 2013.
3. A.B. Neild, SAE Technical Paper 630019 (1963). doi: 10.4271/630019.
4. A.B. Neild, SAE Technical Paper 670452 (1967). doi: 10.4271/670452.
5. U. Birkholz, E. Grob, U. Stohrer, K. Voss, D.O. Gruden, and W. Wurster, in *Proceedings of the 7th International Conference on Thermoelectric Energy Conversion*, Arlington, 1988, pp. 124–128.
6. K. Ikoma, M. Munekiyo, K. Furuya, M. Kobayashi, T. Izumi, and K. Shinohara, in *XVII International Conference on Thermoelectrics, Proceedings ICT 98*, IEEE, 1998, pp. 464–467.
7. E.F. Thacher, B.T. Helenbrook, M.A. Karri, and C.J. Richter, Proceedings of the Institution of Mechanical Engineers. *Proc. Inst. Mech. Eng. Part D: J Automobile Eng.* 221, 95 (2007).
8. E.F. Thacher, B. Helenbrook, and M.A. Karri, in *Proceedings of the DEER Conference*, Detroit, Michigan, 2006.
9. K. Matsubara, in *Twenty-First International Conference on Thermoelectrics, Proceedings ICT'02*, IEEE, 2002, pp. 418–423.
10. K. Matsubara, *MRS Online Proceedings Library*, vol. 691, G2.4 (2001).
11. X.C. Xuan, K.C. Ng, C. Yap, and H.T. Chua, *Int. J. Heat Mass Transf.* 45, 5159 (2002).
12. G. Liang, J. Zhou, and X. Huang, *Appl. Energy* 88, 5193 (2011).
13. C. Baker, P. Vuppuluri, L. Shi, and M. Hall, *J. Electron. Mater.* 41, 1290 (2012).
14. T.J. Hendricks and J.A. Lustbader, in *Twenty-First International Conference on Thermoelectrics, Proceedings ICT'02*, IEEE, 2002, pp. 381–386.
15. N. Espinosa, M. Lazard, L. Aixala, and H. Scherrer, *J. Electron. Mater.* 39, 1446 (2010).
16. S. Kumar, S.D. Heister, X. Xu, J.R. Salvador, and G.P. Meisner, *J. Electron. Mater.* 42, 665 (2013).
17. S. Kumar, S.D. Heister, X. Xu, J.R. Salvador, and G.P. Meisner, *J. Electron. Mater.* 42, 944 (2013).
18. S. Kumar, S.D. Heister, X. Xu, J.R. Salvador, and G.P. Meisner, in *ASME 2012 Summer Heat Transfer*, Rio Grande, Puerto Rico, 2012.
19. R.J. Buist, *CRC Handbook of Thermoelectrics* (Boca Raton: CRC Press, 1995), pp. 143–156.
20. T. Shih and T. Hogan, in *Thermoelectrics Handbook*, ed. by D. Rowe (CRC Press, Boca Raton, 2005), pp. 12–1–12–23.
21. X. Tang, Q. Zhang, L. Chen, T. Goto, and T. Hirai, *J. Appl. Phys.* 97, 093712 (2005).
22. G. Rogl, A. Grytsiv, E. Bauer, P. Rogl, and M. Zehetbauer, *Intermetallics* 18, 57 (2010).
23. C.A. Domenicali, *Phys. Rev.* 92, 877 (1953).